Distributed Nonlinear Compensation Using Optoelectronic Circuits

Benjamin Foo, *Student Member, IEEE*, Bill Corcoran, *Member, IEEE*, and Arthur J. Lowery, *Fellow, IEEE*

(Invited Paper)

***Abstract*—This paper investigates the use of optoelectronic subsystems placed all the way along a fiber link to provide distributed mitigation of the distortion caused by the Kerr nonlinearity. These subsystems use power-dependent phase modulation to mitigate the low-frequency (<1 GHz) components of the self-phase modulation and cross-phase modulation (XPM) distortion experienced by several wavelength channels simultaneously. Furthermore, this technique compensates the nonlinear distortion on a per-span basis, and so can mitigate XPM in optically routed links, unlike transmitter- or receiver-side nonlinearity compensation techniques. We present proof-of-concept results from both experimental and numerical studies that show our optoelectronic technique can effectively mitigate the distortion caused by fiber nonlinearity. Additional simulations study the impact of various link parameters on the effectiveness of this scheme.**

***Index Terms*—Nonlinearity compensation, optical fiber communication, phase modulation.**

I. Introduction

DISTORTIONS caused by the Kerr nonlinearity limit the information capacity of long-haul optical fiber links [1]–[3]. As the Kerr effect is deterministic, techniques that aim to overcome the limitation caused by fiber nonlinearity, i.e., nonlinearity compensation (NLC), have been developed. These techniques can operate on the electrical baseband signal using digital signal processing (DSP) [4]–[22], or directly on the optical signal [23]–[47]. To date, most work on NLC has focused on techniques that use the optical signal at one point of the fiber link to predict the total nonlinear distortion that occurs during transmission, and significant performance improvements have been demonstrated in point-to-point links. For example, digital back propagation (DBP) can take the entire optical signal at either the transmitter or receiver, and use the nonlinear Schrödinger equation (NLSE) to propagate it through a virtual fiber link in order to undo the impairments that are expected to occur during transmission through the physical link [4], [5]. This can improve system reach by a factor of three [48]. However, single-point, or 'lumped', NLC techniques are less effective in systems that employ reconfigurable optical add/drop multiplexers (ROADMs) to perform wavelength routing, since they are unable to accurately compensate the nonlinear distortion caused by wavelength channels that are added or dropped during transmission [6], [49]. One way to overcome the issue of optical routing is to place one (or more) NLC stage(s) between adjacent ROADM nodes [38], [46], [47], [50], so that each stage only compensates the distortion in a fraction of the link. This 'distributed' type of NLC system is more flexible than a 'lumped' approach and can adapt to changes in the signal, but also requires the use of many NLC sub-systems.

The need for multiple stages rules out the use of digital NLC techniques, as they operate on the electrical baseband signal acquired after coherent detection and so require optical-electrical-optical (O-E-O) conversion for each WDM channel; in this case, it may be more advantageous to perform O-E-O regeneration of the signal rather than distributed digital NLC. Therefore, research on distributed NLC has concentrated on all-optical techniques, particularly cascaded optical phase conjugation (OPC) [34]–[41]. This technique utilizes multiple phase conjugation stages placed along a link, and enables better performance than mid-span spectral inversion (MSSI), which only uses a single OPC stage [41]. Further, simulations indicate that cascaded OPC may be more robust to stochastic impairments, such as signal-ASE beating [35], [36] and polarization mode dispersion (PMD) [51], that limit the effectiveness of DBP [52], [53]. Given that OPC can accommodate signals with several THz of optical bandwidth and is compatible with polarization-division multiplexing (PDM) [29], [32], [33], it appears to be an ideal way to combat nonlinear distortions. However, a key factor in using OPC for nonlinear mitigation is the fiber link itself, which should be carefully designed to have symmetric power and dispersion maps around each OPC stage to achieve optimal performance [38], [54], [55]. Another possible all-optical distributed NLC technique is phase-sensitive amplifiers (PSAs) [42], [43], which can perform an optical coherent superposition between a

Manuscript received October 23, 2017; revised November 29, 2017; accepted November 29, 2017. Date of publication December 6, 2017; date of current version March 1, 2018. This work was supported in part by the Australian Research Council's Laureate Fellowship program (FL 130100041), and in part by the ARC Centre of Excellence for Ultrahigh-Bandwidth Devices for Optical Systems (CE 110001018). *(Corresponding author: Benjamin Foo.)*

B. Foo was with the Monash Electro-Photonics Laboratory, Department of Electrical and Computer Systems Engineering, Monash University, Clayton, VIC 3800, Australia. He is now with the Photonics Laboratory, Department of Microtechnology and Nanoscience (MC2), Chalmers University of Technology, Gothenburg SE-412 96, Sweden (e-mail: benjamin.foo@chalmers.se).

B. Corcoran and A. J. Lowery are with the Monash Electro-Photonics Laboratory, Department of Electrical and Computer Systems Engineering, Monash University, Clayton, VIC 3800, Australia, and also with the ARC Centre for Ultrahigh-bandwidth Devices for Optical Systems, Australia (e-mail: bill.corcoran@monash.edu; arthur.lowery@monash.edu).

Color versions of one or more of the figures in this paper are available online at http://ieeexplore.ieee.org.

Digital Object Identifier 10.1109/JLT.2017.2779747

0733-8724 © 2017 IEEE. Translations and content mining are permitted for academic research only. Personal use is also permitted, but republication/redistribution requires IEEE permission. See http://www.ieee.org/publications_standards/publications/rights/index.html for more information.

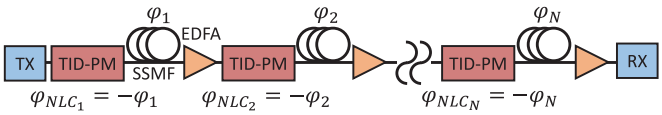

Fig. 1. Block diagram of distributed NLC using in-line TID-PMs. The nonlinear distortion in each fiber span is modeled as a phase rotation, φ_n, which is pre-compensated using a TID-PM.

signal and its phase conjugate to mitigate the nonlinear distortion. However, the need to transmit two copies of the same information greatly reduces spectral efficiency, and the link design requirements are even stricter than for cascaded OPC.

We have previously investigated an alternative distributed NLC technique that uses optoelectronic sub-systems called 'total intensity-directed phase modulators' (TID-PMs) placed before each fiber span in a long-haul link [50], [56]–[58], as illustrated in Fig. 1. Each TID-PM applies a phase rotation that is proportional to the total power of several wavelength-division-multiplexed (WDM) channels to mitigate both self-phase modulation (SPM) and cross-phase modulation (XPM) on a span-by-span basis. A TID-PM can be thought of as an optoelectronic implementation of the nonlinear step in the DBP algorithm, which makes the use of in-line TID-PMs conceptually similar to DBP with one step per span. This technique is compatible with PDM signals using different modulation formats, and is robust to optical routing. Further, TID-PMs can be constructed from commercially available optoelectronic components whose bandwidths are less than the bandwidth of a single wavelength channel. The relatively simple implementation of in-line TID-PMs comes at the cost of reduced accuracy, meaning that ideal DBP or OPC will mitigate the nonlinear distortion more effectively than optimized in-line TID-PMs. However, as we will show in this paper, in-line TID-PMs are able to offer comparable performance to practical implementations of DBP, e.g., single-channel DBP with one step per span [50].

In this paper, which is an extension of an invited presentation at ECOC 2017 [59], we review progress on in-line TID-PMs, and present new simulation results that investigate the performance penalty for using TID-PMs with sub-optimal parameters. We also discuss several open questions regarding the use of in-line optoelectronic sub-systems for NLC, and highlight areas where improvements may be possible. The rest of this paper is organized as follows: Section II describes the theory enabling XPM compensation using TID-PMs, and the approximations that can be made to simplify TID-PM design. In Section III, numerical simulations are used to explore in-line TID-PMs in different transmission systems, and briefly investigate the impact of various system parameters. A proof-of-concept experiment is then presented in Section IV, where in-line TID-PMs are used in a long-haul WDM link. Section V then discusses our findings, and Section VI concludes the paper.

II. Total Intensity-Directed Phase Modulators

The use of power-dependent phase rotations to mitigate the Kerr nonlinearity is derived from the numerical models that describe how an electromagnetic wave propagates through an optical fiber. In a randomly birefringent optical fiber with negligible PMD, signal propagation can be described using the Manakov-PMD approximation of the NLSE [60], [61]:

$$\frac{\partial \mathbf{E}}{\partial z} + \frac{\alpha}{2}\mathbf{E} + j\frac{\beta_2}{2}\frac{\partial^2 \mathbf{E}}{\partial t^2} = j\gamma\frac{8}{9}(|\mathbf{E}|^2)\mathbf{E} \tag{1}$$

where $\mathbf{E} = [E_x, E_y]^T$ is the vector for the time-varying electric fields of the signal in the X and Y polarizations, $j = \sqrt{-1}$, and α, β_2 and γ are the attenuation co-efficient, group velocity dispersion (GVD) parameter and nonlinear co-efficient of the fiber, respectively. The terms on the left-hand side describe the linear response of the optical fiber, while the term on the right-hand side describes how the Kerr nonlinearity affects the signal. In the absence of GVD (i.e., $\beta_2 = 0$), the power-dependent phase rotation caused by the Kerr effect can be approximated as [62]:

$$\phi_{NL} = \gamma\frac{8}{9}L_{eff}(|E_x|^2 + |E_y|^2), \tag{2}$$

where L_{eff}, the nonlinear effective length, is given by:

$$L_{eff} = \frac{1 - \exp(-\alpha L)}{\alpha}, \tag{3}$$

for a fiber span of length L. Therefore, applying a phase rotation of equal magnitude, but in the opposite direction, should perfectly mitigate this distortion. This concept has been considered in several previous studies, where a single phase rotation was performed at the end-points of a link [23]–[26]. However, most long-haul links use fiber that is highly dispersive (i.e., $\beta_2 \neq 0$). In these systems, the nonlinear distortion cannot be accurately modeled as a simple phase rotation because GVD changes the shape of the optical waveform during transmission [6], [25]. Moreover, higher-order nonlinear mixing terms, e.g., four-wave mixing (FWM) and cross-polarization modulation (XpolM), cannot be fully modeled in as simple a manner as (2). Properly describing the interaction between the Kerr nonlinearity and GVD requires the use of iterative techniques, e.g., the split-step Fourier method [63], that divide the link into many segments and solve the NLSE for each one. To accurately model nonlinear propagation, the step size should be chosen such that the nonlinear distortion in each segment is small, and so the linear and nonlinear parts of the NLSE can be solved separately; the solution to the linear portion of the NLSE for a segment is perturbed by the power-dependent phase rotation given by the nonlinear portion. Therefore, the Kerr nonlinearity can, in theory, be compensated by performing multiple phase rotations that are dependent on the signal power at different points along the link. This is the general principle behind DBP [4]–[6], and can also be emulated using optoelectronic sub-systems, such as TID-PMs, placed along the fiber link.

An interesting problem is how to physically measure all of the intensity fluctuations for a broadband optical signal multiple times along a transmission link. The use of WDM means that the optical signal can occupy several THz of bandwidth, and measuring the power of the electric field directly would require a photodiode with twice the full optical bandwidth in order to capture the high-frequency mixing products. This is not feasible with optoelectronic components. One way to overcome this

problem is to consider the distortion experienced by a single channel in a WDM signal. When viewed in this way, the overall distortion on each wavelength channel can be divided into contributions from SPM, XPM, non-degenerate FWM, and XpolM. Of these, SPM and XPM are the dominant impairments in most long-haul systems; non-degenerate FWM is generally inefficient in dispersive fibers and can be ignored [62], [64], and previous studies have shown that XpolM is less significant than either SPM or XPM for many transmission systems [65]–[67]. The distortion caused by SPM and XPM on the ith channel is [68]:

$$\begin{aligned}\phi_{NL,ix}(t) &= \gamma\frac{8}{9}L_{eff}\left(|E_{ix}|^2+|E_{iy}|^2\right)\\ &\quad+\gamma\frac{8}{9}L_{eff}\sum_{j\neq i}\left(2|E_{jx}|^2+|E_{jy}|^2\right),\\ \phi_{NL,iy}(t) &= \gamma\frac{8}{9}L_{eff}\left(|E_{ix}|^2+|E_{iy}|^2\right)\\ &\quad+\gamma\frac{8}{9}L_{eff}\sum_{j\neq i}\left(2|E_{jy}|^2+|E_{jx}|^2\right),\end{aligned}\tag{4}$$

where $|E_{i\{x,y\}}|^2$ is the power in the X- or Y-polarization tributary of the ith WDM channel. This indicates that phase rotations that are proportional to the weighted sum of the power in each channel can mitigate the Kerr nonlinearity, trading the need for a single photodiode with multiple THz of bandwidth for many photodiodes with bandwidths in the 10's of GHz. Further, the GVD of the fiber results in WDM channels 'walking-off' from each other and so the XPM distortion between channels that have a large difference in group velocity is small [69]. This reduces both the number of channels that need to be detected, and the bandwidth of the photodiodes.

Chiang *et al.* [70], [71] analytically derived an expression to describe how walk-off affects the XPM distortion caused to a continuous wave (CW) tone by an intensity-modulated WDM channel, referred to as the 'pump'. This 'XPM transfer function' assumes that the XPM distortion can be described as a small perturbation of the linear solution to the NLSE, where the perturbation is a phase rotation that is dependent on an 'average' waveform of the pump. Following this analysis, the XPM distortion for a single-polarization signal with co-polarized channels propagating through one fiber span is [70], [71]:

$$\phi_{XPM} = 2\gamma L_{eff}|E_{XPM}|^2 \otimes IFT\left\{\eta_{XPM(\omega)}\right\},\tag{5}$$

where IFT $\{.\}$ is the inverse Fourier transform, $\otimes$ represents the convolution operation, $|E_{XPM}|^2$ is the power waveform of the pump channel, ω is the angular modulation frequency of the pump channel at the electrical baseband, and $\eta_{XPM(\omega)}$, the XPM transfer function, is modeled as a filter acting on the optical power waveform of the interfering channel (i.e., $|E_{XPM}|^2$), described by:

$$|\eta_{XPM}(\omega)| = \sqrt{\frac{\alpha^2}{\omega^2 d^2+\alpha^2}\left[1+\frac{4\sin^2(\frac{\omega dL}{2})\mathrm{e}^{-\alpha L}}{(1-\mathrm{e}^{-\alpha L})^2}\right]},\tag{6}$$

for the filter magnitude and:

$$\begin{aligned}\angle\eta_{XPM}(\omega) &= \tan^{-1}\left(\frac{\mathrm{e}^{-\alpha L}\sin(\omega dL)}{\mathrm{e}^{-\alpha L}\cos(\omega dL)-1}\right)\\ &\quad-\tan^{-1}\left(\frac{\omega d}{-\alpha}\right),\end{aligned}\tag{7}$$

for the filter phase, where L is the length of the fiber, α is the attenuation, and d is the walk-off parameter:

$$d=\int_{\lambda_{XPM}}^{\lambda_{CW}} D(\lambda)d\lambda,\tag{8}$$

where λ_{XPM} is the wavelength of the pump channel, λ_{CW} is the wavelength of the CW tone, and $D(\lambda)$ describes how the dispersion of the fiber varies with wavelength. When considering dispersive fiber with channels placed away from the zero-dispersion wavelength, (8) can be approximated by $d\approx D(\lambda_{CW}-\lambda_{XPM})=D\Delta\lambda$. This analysis has been refined to include PDM signals [72], and dependence on pulse shape and dispersion map [73]. The physical effect of the filter is to transform the waveform of the interfering channel at the start of the span into the average waveform that causes the XPM distortion. Using the XPM transfer functions for several WDM channels has been explored as a way to simplify full-field DBP [12], [68], [74], [75], and we briefly looked at implementing this in optoelectronics [56]. An additional consideration is that the contributions of each spectral component from different spans add coherently [76], which creates nulls in the magnitude response of the XPM transfer function of multi-span links. The magnitude of the overall XPM transfer function for a periodically amplified link without in-line dispersion management is given by [71]:

$$\eta_{Link}(\omega)=\left|\frac{\sin\left(\frac{N\omega dL}{2}\right)}{\sin\left(\frac{\omega dL}{2}\right)}\right|\times|\eta_{XPM}(\omega)|,\tag{9}$$

where N is the number of spans. To illustrate this, we plot (9) with $N=1$ and $N=20$ in Fig. 2. Clearly, walk-off attenuates the XPM distortion caused by high-frequency intensity fluctuations in a single span [Fig. 2(a)], and these components are attenuated further due to the coherent addition that takes place in multi-span links [Fig. 2(b)]. This indicates that the majority of the XPM distortion experienced at the end of a long-haul link is caused by relatively low-frequency (<1 GHz) spectral components [27], [28], [76]. Additionally, studies on filtered DBP [9], [10] have demonstrated that SPM is similarly dominated by low-frequency components. Therefore, it may be possible to achieve significant performance improvement by only compensating the nonlinear distortion caused by low-frequency intensity fluctuations, and letting walk-off suppress everything else. This approach will not perfectly compensate the nonlinear distortion, but does suggest that devices with ultra-high bandwidths are not required for effective nonlinearity mitigation.

With this idea in mind, we developed an optoelectronic subsystem called a 'total intensity-directed phase modulator' (TID-PM) [50], [56]–[58], that aims to mitigate SPM and XPM using low-bandwidth components. The block diagram of a TID-PM is

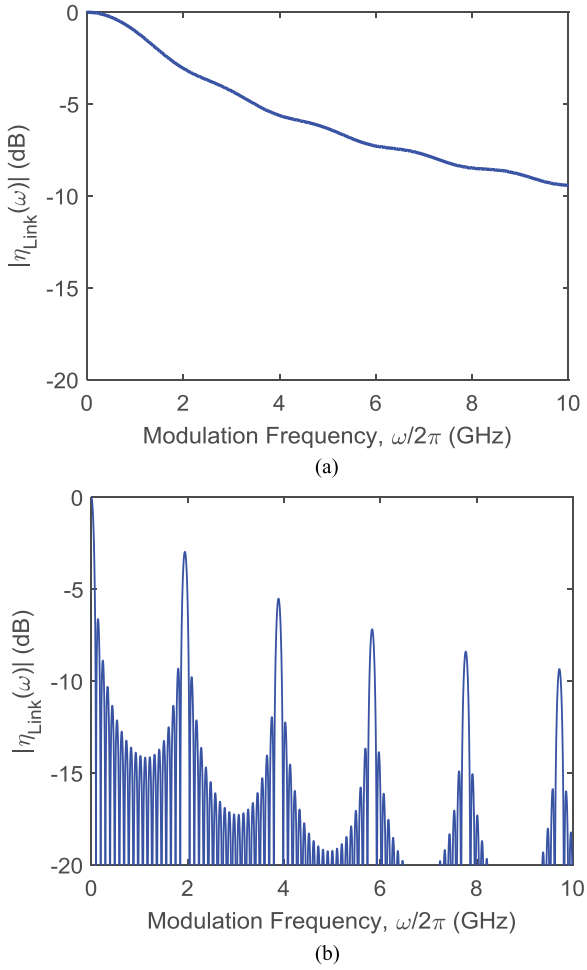

Fig. 2. Magnitude of the XPM transfer function after (a) 1 span and (b) 20 spans. Curves are plotted using (9) assuming: channels with 0.4-nm (50-GHz) spacing, and 80-km fiber spans with D = 16 ps · nm^{-1} · km^{-1}, and $\alpha = 0.2$ dB/km.

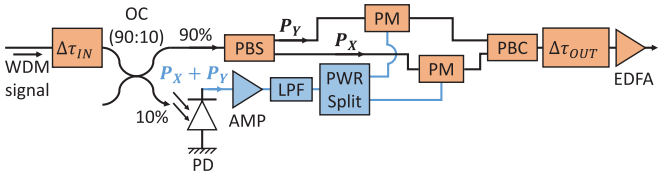

Fig. 3. Block diagram of a TID-PM. $\Delta\tau_{IN/OUT}$: Channel-wise optical group delay elements; OC: Optical coupler with 90%/10% splitting ratio; PD: Photodiode; AMP: Electrical amplifier; LPF: Electrical low-pass filter; PWR split: 3-dB electrical power splitter; PBS: Polarization beam splitter; PM: Phase modulator; PBC: Polarization beam combiner.

given in Fig. 3. This is very similar to sub-systems previously developed for receiver-side compensation of SPM [23] and XPM [27], [28]. The core of this idea is to use an optical coupler to tap off a portion of the total power in a WDM signal, which is then measured using a photodiode. The electrical signal is then amplified, and used to drive a phase modulator to apply a phase rotation that has the same magnitude but opposite direction to the phase rotation caused by the Kerr effect. In this case, we emulate a polarization-insensitive phase modulator by dividing the

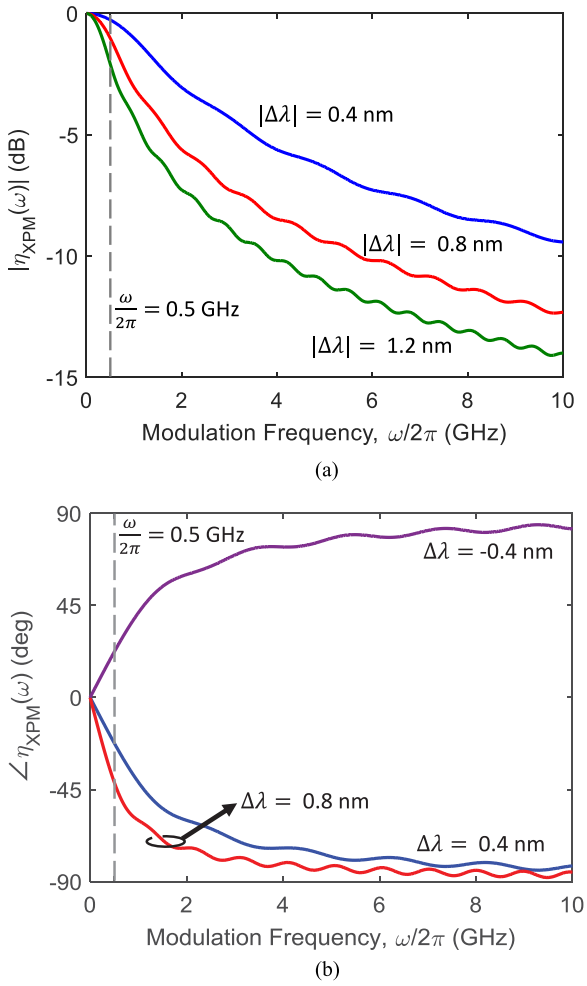

Fig. 4. (a) The magnitude response of the XPM transfer functions for channels with 0.4- (blue), 0.8- (red), and 1.2-nm (green) wavelength separation. (b) Phase response of the XPM transfer functions for channels with 0.4- (blue), 0.8- (red), and -0.4-nm (purple) wavelength separation. Curves are plotted using (6) and (7) assuming: L = 80 km, D = 16 ps · nm^{-1} · km^{-1}, and $\alpha = 0.2$ dB/km.

signal into orthogonal polarization tributaries using a polarization beam splitter (PBS), modulating both tributaries separately, and then re-combining them using a polarization beam combiner (PBC). In order to enable XPM compensation, elements to emulate the magnitude and phase response of the XPM transfer functions need to be added. In this case, we have chosen to use an electrical low-pass filter (LPF) for the magnitude response, and a channel-wise optical group delay, $\Delta\tau_{IN}$, for the phase response. To justify these decisions, we plot the magnitude and phase responses of the XPM transfer functions for pairs of WDM channels with several wavelength separations in Fig. 4. Fig. 4(a) plots the magnitude response of the XPM transfer functions for channels with 0.4-, 0.8-, and 1.2-nm separation. While the XPM transfer functions for high-frequency components are different, all the XPM transfer functions are quite similar at low modulation frequencies (e.g., below 500 MHz). Therefore, a LPF that matches this part of the response can be applied to several WDM channels, and the same phase rotation can be used to mitigate the SPM and XPM distortions on these channels. We also plot

the phase response of the XPM transfer functions for interferers with carrier wavelengths that are 0.4-nm above, 0.8-nm above, and 0.4-nm below λ_{CW} in Fig. 4(b). The low-frequency components of the phase responses are almost linear, which indicates a constant group delay. This makes physical sense, since the difference in group velocity between channels means that the average nonlinear waveform should delay channels relative to each other. We note that Fig. 4(b) appears to require a negative group delay (i.e., the signal needs to be advanced in time) when the interfering channel is centered on a carrier 0.4 nm below the channel being distorted. What this physically means is that a symbol currently entering the fiber span will, on average, be distorted by a symbol on the interfering channel that has not yet reached the beginning of the span. This is consistent with propagation in a medium with anomalous GVD, where light with longer wavelengths travel slightly faster than light with shorter wavelengths [62]. Setting the channel-wise group delays relative to the shortest-wavelength channel in the WDM band avoids the need for a 'negative' delay. Additionally, the time mis-alignment introduced by $\Delta\tau_{IN}$ must be undone before the TID-PM output, since the average waveform is determined by the input to the fiber, not the input to the TID-PM. Therefore, a second channel-wise optical group delay, $\Delta\tau_{OUT}$, is added. Because the optoelectronic components attenuate the signal, an Erbium-doped fiber amplifier (EDFA) is used just before the TID-PM's output to perfectly recover the overall insertion loss. This also reduces the TID-PM's effective noise figure.

III. Numerical Simulations

In this section, we present the results of several numerical simulations that investigate how some parameters of the fiber link and the TID-PM sub-system affect nonlinearity mitigation. VPItransmissionMaker was used to simulate several scenarios where signals employing both WDM and PDM are transmitted through dispersion unmanaged links with TID-PMs placed before each fiber span, as shown in Fig. 1. In all cases, we considered the transmission of an 8-channel, 28-Gbaud PDM-16QAM signal. MATLAB was used to generate random binary data for both polarization components of all eight channels, which was then mapped onto 16QAM symbols using Gray coding. The symbols were then upsampled to two-samples-per-symbol and shaped with a root-raised cosine (RRC) filter with 0.01 roll-off before being imported into the simulation engine. The simulations considered 2^{15} symbols, and each symbol was represented in the optical domain with 16-times oversampling. The symbols were modulated onto lasers with 100-kHz linewidths using complex Mach-Zehnder modulators (C-MZMs) and multiplexed together before being launched into the transmission link. We considered channels that were placed on a 30-GHz, or a 50-GHz frequency grid. While we investigated links with different lengths, they all used 100-km spans of standard single-mode fiber (SSMF), which was modeled with the parameters in Table I. EDFAs with a 6-dB noise figure (NF) were used to recover all losses. After transmission, the channel of interest was de-multiplexed using a 2nd-order Gaussian bandpass filter with 40-GHz bandwidth, and coherently received. The local

TABLE I
Parameters Used for Numerical Simulations in Section III

Parameter	Value
Attenuation (α)	0.2 dB/km
Dispersion	16 ps·nm^{-1}·km^{-1}
Nonlinearity (γ)	1.3 W^{-1}·km^{-1}
PMD	0.05 ps·km$^{-0.5}$
A_{eff}	80 μm^2
Span Length	100 km
EDFA NF	6 dB

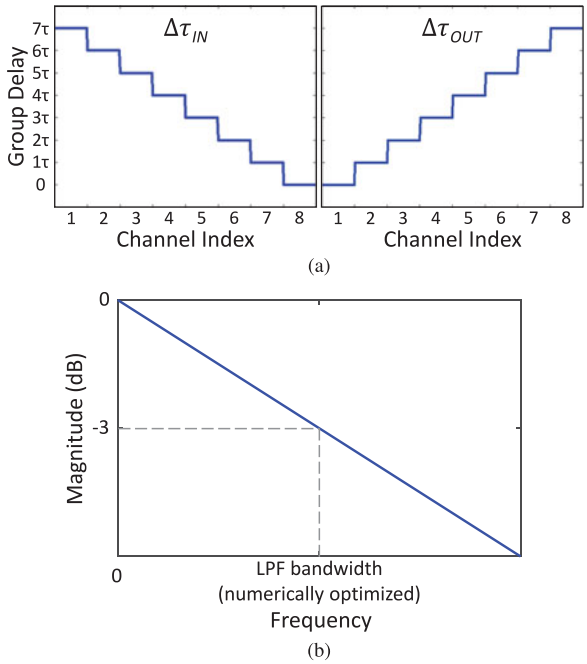

Fig. 5. (a) Group delay profiles of the $\Delta\tau_{IN}$ and $\Delta\tau_{OUT}$ optical filters used to implement the phase response of the XPM transfer function. The channel with the lowest carrier frequency is assigned an index of 1. (b) Frequency response of the LPF used to implement the magnitude response of the XPM transfer function. The values of the 3-dB LPF bandwidth and the delay between adjacent WDM channels, τ, were optimized using numerical sweeps.

oscillator was assumed to have a linewidth of 100 kHz. DSP techniques were then applied to the received signal. Dispersion was compensated using the overlap-add algorithm, and the signal was equalized using a least-mean-squared (LMS) dynamic equalizer. Laser phase noise was recovered using a maximum-likelihood algorithm, and then the number of bit errors was counted directly. Finally, the system performance, Q, was calculated from the bit error rate (BER) using [62]:

$$Q_{\mathrm{BER}}\,(\mathrm{dB}) = 20\,\log_{10}\left(\sqrt{2}\mathrm{erfc}^{-1}(2\mathrm{BER})\right), \qquad (10)$$

where erfc^{-1} is the inverse of the complementary error function.

The in-line TID-PMs were modeled using the block diagram shown in Fig. 3. The phase response of the XPM transfer function is modeled using an optical filter, $\Delta\tau_{IN}$, that applies a different group delay to each channel as shown in Fig. 5(a). The signal power is then split using a 90:10 optical coupler, and the total power (i.e., the power in both polarizations of all eight

channels) out of the 10% arm is detected using a photodiode. The signal is electrically amplified, and a LPF with the profile in Fig. 5(b), i.e., a 0.5-order Gaussian, was used to emulate the low-frequency component of the magnitude response of the XPM transfer function. This filter profile is optimal for SPM compensation [77]. For a 50-GHz grid spacing we find that in-line TID-PMs perform optimally with a 0.75-GHz bandwidth LPF and when τ, the group delay between adjacent channels, is 50 ps. When the spacing is reduced to 30 GHz, the optimal LPF bandwidth increases to 1.3 GHz and the optimal value of τ becomes 30 ps. The output from the LPF is then split into two identical signals, and used to drive two phase modulators. In the optical arm, the 90% output from the optical coupler passes through what is effectively a polarization-insensitive phase modulator to remove the nonlinear distortion. The $\Delta\tau_{OUT}$ optical filter applies additional delays to re-align the symbols to their relative positions at the TID-PM input, and then an EDFA with 6-dB NF recovers the insertion loss of the TID-PM. In all simulations, we model the TID-PM with an insertion loss of 5.5 dB, where we assume commercially available ultra-low loss phase modulators with 2-dB insertion loss, a 0.5-dB loss over an ideal 90:10 coupler, and a 3-dB combined loss for the $\Delta\tau_{IN}$ and $\Delta\tau_{OUT}$ elements. We can estimate the optical signal-to-noise ratio (OSNR) penalty from the TID-PM's loss by comparing the effective noise figure of a span with and without a TID-PM. Using the cascaded amplifier formula, the noise figure for a span without in-line TID-PMs is:

$$NF_{Uncomp} = NF_{SSMF} + \frac{NF_{EDFA} - 1}{G_{SSMF}}, \tag{11}$$

where NF_{SSMF} is the noise figure of the span of SSMF, NF_{EDFA} is the EDFA noise figure, and G_{SSMF} is the 'gain' in the SSMF. Because SSMF attenuates the signal, $NF_{SSMF} = L_{SSMF}$ and $G_{SSMF} = 1/L_{SSMF}$, where L_{SSMF} is the total loss of the fiber. Similarly, the noise figure of a span with in-line TID-PMs is:

$$\begin{aligned} NF_{NLC} = {} & NF_{TID-PM} + \frac{NF_{EDFA} - 1}{G_{TID-PM}} \cdots \\ & + \frac{NF_{SSMF} - 1}{G_{TID-PM} G_{EDFA,TID-PM}} \cdots \\ & + \frac{NF_{EDFA} - 1}{G_{TID-PM} G_{EDFA,TID-PM} G_{SSMF}}, \end{aligned} \tag{12}$$

where NF_{TID-PM} and G_{TID-PM} are the noise figure and gain of the TID-PM, and $G_{EDFA,TID-PM}$ is the gain of the EDFA at the TID-PM output. The terms related to the TID-PM precede the SSMF terms because the TID-PM is inserted before the fiber span (see Fig. 1). As with the SSMF, $NF_{TID-PM} = L_{TID-PM}$ and $G_{TID-PM} = 1/L_{TID-PM}$, where L_{TID-PM} is the insertion loss of the TID-PM. Additionally, $G_{EDFA,TID-PM} = L_{TID-PM}$ since this EDFA perfectly recovers the loss of the TID-PM. Substituting the values used in the simulation (SSMF loss of 20 dB, EDFA noise figure of 6 dB, TID-PM loss of 5.5 dB), NF_{Uncomp} is 26 dB while NF_{NLC} is 26.14 dB, and so the estimated OSNR penalty from inserting in-line TID-PMs is 0.14 dB. We note that TID-PMs with a 5.5-dB insertion loss is quite optimistic, and that an insertion loss closer to 7.5 dB is more realistic (see Section V). However, the estimated OSNR penalty for using in-line TID-PMs with 7.5-dB loss is still only 0.23 dB, and we do not expect the 0.1-dB difference in OSNR to greatly affect performance at the optimum launch power.

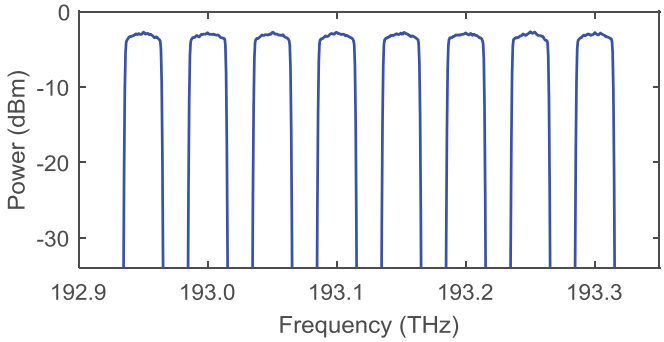

Fig. 6. Optical spectrum of the simulated 8 × 28 Gbaud PDM-16QAM signal on a 50-GHz grid.

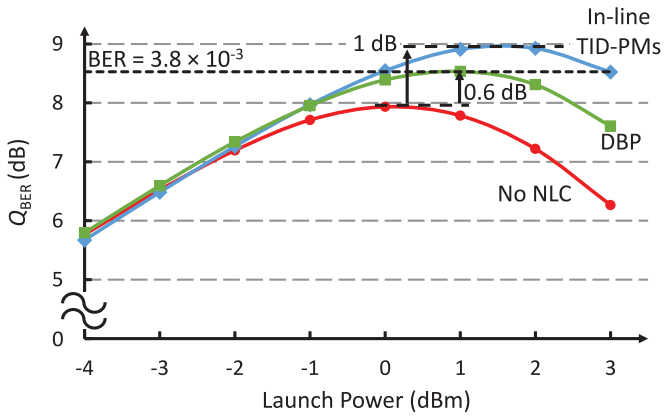

Fig. 7. Simulated Q_{BER} *vs.* per-channel launch power for a central PDM-16QAM channel after transmission through a 15 × 100-km link. The curves compare systems with no NLC (red circles), single-channel DBP with one step per span (green squares), and in-line TID-PMs (blue diamonds). From [50].

A. Nonlinearity Mitigation Using In-Line TID-PMs

We first consider channels placed on a standard 50-GHz grid transmitted through a 15 × 100-km link. The optical spectrum of this signal is shown in Fig. 6. Fig. 7 plots Q_{BER} *vs.* per-channel launch power for the channel centered on 193.1 THz, comparing the system performance with no NLC (red circles), i.e., only compensating linear transmission impairments, and with in-line TID-PMs (blue diamonds). Inserting TID-PMs into the link increases the optimum launch power from 0 dBm to 1 dBm, and enables an improvement to peak Q_{BER} of 1 dB. To reference the performance improvement to a known NLC technique, we also plot a curve for single-channel DBP (green squares), implemented using the asymmetric split-step Fourier method [4] and one step per span. In-line TID-PMs enable a slightly larger increase in peak Q_{BER} than single-channel DBP, which is because they can partially mitigate XPM in addition to SPM.

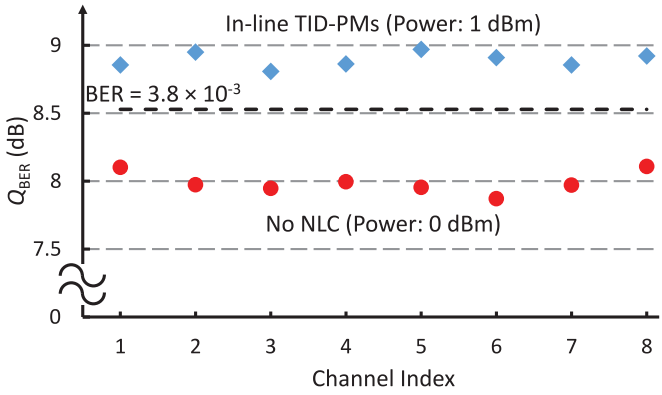

Fig. 8. Simulated Q_{BER} *vs.* channel index for PDM-16QAM signal with (blue) and without (red) NLC from in-line TID-PMs. Q_{BER} is determined at the optimum launch power for each system. From [50].

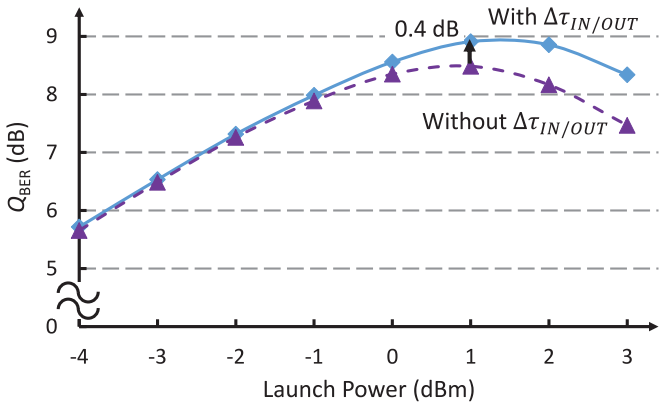

Fig. 9. Q_{BER} *vs.* launch power for in-line TID-PMs with (blue) and without (purple) optical group delay elements.

To confirm that in-line TID-PMs can mitigate both SPM and XPM, Fig. 8 plots Q_{BER} for all eight channels. These channels were measured at the optimum launch power, which was 0 dBm for the link without NLC (red circles) and 1 dBm for the link with in-line TID-PMs (blue diamonds). The performance of all eight channels is improved by between 0.8 dB and 1 dB. Further, we note that the edge channels in the link without NLC perform slightly better than the central channels, since they only experience XPM from one side [78], while all channels achieve similar performance in the link employing in-line TID-PMs. This indicates that in-line TID-PMs mitigate both SPM and XPM.

B. Sub-Optimal In-Line TID-PMs

Using the above results as a baseline, we then performed numerical sweeps of several internal TID-PM parameters to see how sub-optimal operating conditions affect their nonlinearity mitigation efficacy. We first considered whether the optical delays, $\Delta\tau_{IN/OUT}$, are necessary. Fig. 9 plots Q_{BER} *vs.* launch power per channel for the link where in-line TID-PMs included the optical delay elements (blue diamonds), and when these optical delays were removed (purple triangles). All other

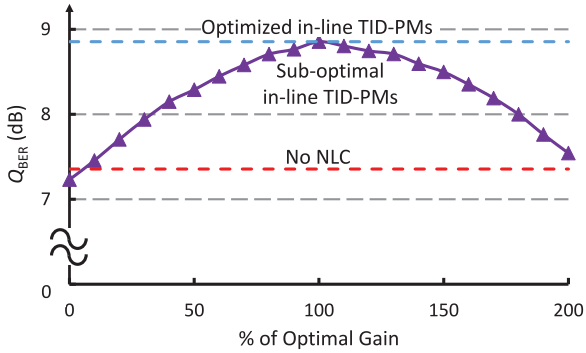

Fig. 10. Q_{BER} of a central PDM-16QAM channel as the gain of the electrical amplifier is varied from 0% to 200% of the optimum value. The per-channel launch power is 2 dBm.

simulation parameters remained the same. A 0.4-dB penalty at the optimum launch power is observed when the delays were not used, putting it on par with the DBP result in Fig. 7. This clearly demonstrates the need to accurately model the phase response of the XPM transfer function.

Another important parameter is the amplification of the electrical signal (i.e., the gain of the electrical amplifier, AMP, in Fig. 3), which determines the phase modulation depth. The optimum gain can be calculated from:

$$G = \left(\frac{1}{aR}\right)\gamma L_{eff}\left(\frac{V_\pi}{\pi}\right), \tag{13}$$

where a is the fraction tapped off by the optical coupler (in this case, 0.1), R is the responsivity of the photodiode, and V_π is the voltage swing that results in a 180-degree phase rotation when applied to the phase modulator. Fig. 10 plots Q_{BER} against the percentage of the optimum gain (purple triangles) for a launch power of 2 dBm per channel. This operating point was chosen to ensure that the system was in the nonlinear region and so the effectiveness of the NLC is clearly reflected in Q_{BER} i.e., a sub-optimal gain would cause a noticeable performance penalty. The Q_{BER} of links without NLC (red) and with optimized in-line TID-PMs (blue) are also plotted as a reference. When the gain is set to zero, none of the nonlinear distortion is mitigated and performance is slightly worse than when no in-line TID-PMs are used. This is expected because the insertion loss of each TID-PM causes a small OSNR penalty. As the electrical gain is increased towards the optimum value, performance steadily improves until the optimal performance is achieved. However, increasing the gain beyond this point results in performance penalties as the nonlinear distortion is overcompensated; when the gain is 200% of the optimum value, there is virtually no performance improvement. Similar behavior was previously observed by Kikuchi [26]. Concentrating on the region around the optimal operating point, the performance penalty is less than 0.1 dB for gains between 90% and 110% of the optimum.

The importance of the path-matching between the optical and electrical arms of the TID-PM was also investigated. The launch power per channel was again set to 2 dBm, and a relative delay was introduced between the two arms, which was swept from

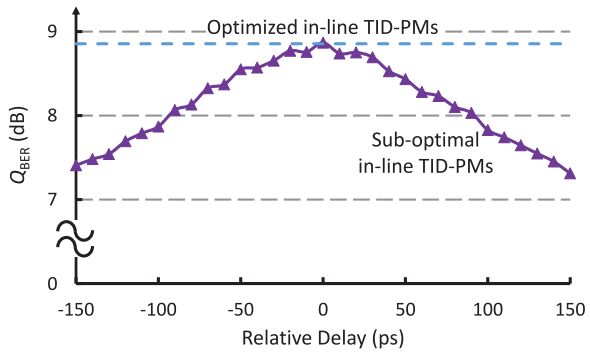

Fig. 11. Q_{BER} of a central PDM-16QAM channel *vs.* the relative delay caused by path-length mismatch between electrical and optical arms for per-channel launch power of 2 dBm. Negative relative delay indicates that the optical pulse arrives at the phase modulator before the corresponding electrical pulse.

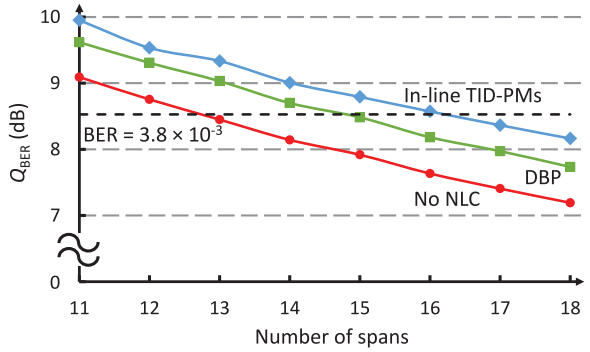

Fig. 12. Q_{BER} *vs.* distance for a central channel of the PDM-16QAM signal with various NLC schemes at the optimum launch power. From [50].

−150 ps (the optical pulse arrives at the phase modulator first) to +150 ps (the electrical pulse arrives at the phase modulator first). The results of this sweep are plotted in Fig. 11. The optimum performance is obtained when the signals are perfectly synchronized, as expected, and there is a clear performance penalty that grows with the path-length mismatch. In this case, the performance penalty was less than 0.1 dB for delays less than 20 ps, which corresponds to 56% of the symbol period. This result, in combination with the result from Fig. 10, indicates that in-line TID-PMs are robust to small errors within the sub-system, which is an important consideration for physical implementation.

C. Sensitivity to Link Parameters

We performed additional simulations to investigate how several link parameters can affect in-line TID-PMs. First, we investigated the maximum reach improvement enabled by in-line TID-PMs. Fig. 12 plots Q_{BER} *vs.* the number of 100-km spans for each of the same systems as Fig. 7. Each curve is plotted for the optimum launch power per channel, which was 0 dBm for the link without NLC, 1 dBm for the link using DBP, and 1 dBm for the link with in-line TID-PMs. We consider the reach of each system to be the maximum distance that its BER is below 3.8×10^{-3}, which corresponds to a common 7% hard-decision forward error correction (HD-FEC) threshold [2]. For this criteria, the link without NLC has a reach of 1200 km, DBP increases the reach to 1400 km, and in-line TID-PMs enable an increase to 1600 km. Note, however, that with slightly different pre-FEC thresholds, the improvement in reach between these systems will vary by one or two spans. Additionally, comparing the values of Q_{BER} for each distance in Fig. 12 shows that in-line TID-PMs enable about the same performance improvement regardless of system length. This is expected, since the number of spans should not greatly impact performance when NLC occurs on a per-span basis.

To determine if in-line TID-PMs are affected by optical routing, we shortened the link to 14×100 km, and placed ROADMs at various points. At each ROADM node, the 8-channel 28-Gbaud PDM-16QAM signal with 50-GHz spacing, was demultiplexed and seven of the eight channels were dropped. Seven new channels were then multiplexed with the one remaining channel so that only the fourth channel (centered on 193.1 THz) was transmitted through the entire link. The multiplexers and de-multiplexers in all ROADMs were modeled with 4th-order Super-Gaussian filters with 40-GHz bandwidth. Fig. 13 plots Q_{BER} *vs.* per-channel launch power for the fourth channel with (a) 0 ROADMs in the link (point-to-point link), (b) 1 ROADM placed at the mid-point of the link (after span 7), and (c) 4 ROADMs placed after spans 1, 5, 9, and 13. In-line TID-PMs enable similar performance improvements in all three cases, indicating a robustness to optical routing. We expect that this is due to the ability of the TID-PMs to compensate for some part of the XPM distortion on a span-by-span basis. This is indicated here by in-line TID-PMs outperforming single channel DBP (i.e., SPM mitigation) in Fig. 7.

Finally, we investigated how the effectiveness of in-line TID-PMs is affected by reducing the channel spacing. We placed the eight channels on a 30-GHz grid, as shown in Fig. 14, which reduced the guard-band to less than 10%. After optimization using numerical sweeps, the bandwidth of the TID-PM's LPF was changed to 1.3 GHz, and τ was set to 30 ps per channel. Fig. 15 plots Q_{BER} *vs.* launch power per channel for this case, again comparing systems with no NLC (red circles), one-step-per-span single-channel DBP (green squares), and in-line TID-PMs (blue diamonds). For this reduced channel spacing, both DBP and in-line TID-PMs are less effective. We attribute this to the reduced walk-off between channels resulting in stronger XPM distortions that are imperfectly compensated. However, in-line TID-PMs still enable a 1-dB increase in optimum launch power and a 0.6-dB improvement in peak Q_{BER}, which is slightly better than DBP.

IV. Experimental Demonstration

We also performed a proof-of-concept experiment, demonstrating in-line TID-PMs in a long-haul transmission system. This was first reported in [58]. The setup for this experiment is shown in Fig. 16. First, we built a TID-PM prototype using commercially available bulk optical components. The input delay, $\Delta\tau_{IN}$, was implemented using a 10-km spool of SMF-28e, and then an EDFA amplified the signal to the power level

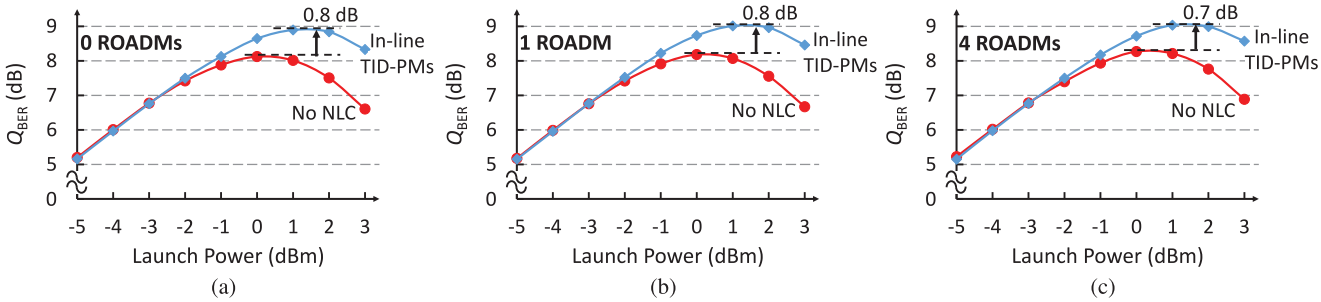

Fig. 13. Q_{BER} *vs.* launch power for 14 × 100-km links with (a) 0 ROADMs, (b) 1 ROADM (after span 7) and (c) 4 ROADMs (after spans 1, 5, 9, and 13).

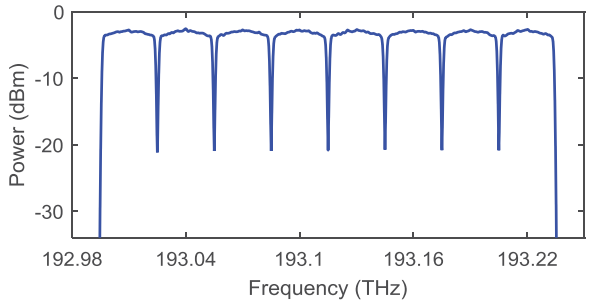

Fig. 14. Optical spectrum of the simulated 8 × 28 Gbaud PDM-16QAM signal on a 30-GHz grid.

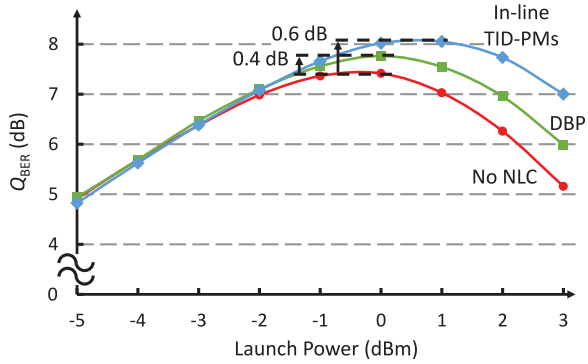

Fig. 15. Simulated Q_{BER} *vs.* per-channel launch power for a central PDM-16QAM channel after transmission through a 15 × 100-km link, when the channels are placed on a 30-GHz grid.

that would be launched into the link. After the EDFA, a 90:10 optical coupler was used to tap off a small portion of the signal, and the power out of the 10% port was measured using a photodiode with 10-GHz bandwidth. A fixed-gain electrical amplifier was combined with a voltage-controlled attenuator to boost the detected intensity waveform to the desired level before low-pass filtering. The LPF was a Mini-circuits SBLP-1870+, the measured frequency response and group delay profile of which are given in Fig. 17(a) and (b), respectively. This filter was chosen because it is a good approximation of the XPM transfer function between channels with 50-GHz separation [71] [Fig. 17(a), green line] up to around 1.7 GHz. A variable electrical delay line matched the length of the optical and electrical paths, and then a power splitter divided the signal so that both phase modulators applied the same phase rotation. A switch that could disable NLC by disconnecting the drive signal to the phase modulators was also added to assist performance comparisons. In the optical arm, the 90% output from the coupler was split into orthogonal polarizations using a PBS. Each tributary was phase modulated to suppress the nonlinear distortion, and then re-combined with a PBC. Both phase modulators had insertion losses of 3.4 dB. Because the output pigtail of the phase modulators used in this prototype were not polarization-maintaining, the inputs to the PBC were manually aligned using fiber-based polarization controllers. Optical delay lines were also added between the phase modulators and polarization controllers to ensure that the path lengths of the two optical arms were matched. A length of dispersion compensating fiber (DCF) designed to compensate 20 km of SMF-28e and a second 10-km spool of SMF-28e were used to implement $\Delta\tau_{OUT}$. The insertion loss of this prototype, measured between Point 1 and Point 2 in Fig. 16, was 11.2 dB, and this was recovered by an EDFA just before the TID-PM's output. This prototype was then placed in a recirculating loop with an 80-km span of SMF-28e (ITU G.652) to emulate a 10 × 80-km dispersion unmanaged link with in-line NLC. The loss of the fiber was recovered using another EDFA, and a wavelength-selective switch (WSS) with 1-THz bandwidth removed out-of-band amplified spontaneous emission (ASE) noise. A polarization scrambler was also placed in the loop to ensure that the state of polarization was changed between measurements.

The transmitted signal was 5 channels of 28-Gbaud PDM-16QAM, placed on a 50-GHz grid. MATLAB was used to generate the data for 2^{17} 16QAM symbols, and the waveform was up-sampled to 90 GSa/s before being stored on an arbitrary waveform generator (AWG) with 33-GHz bandwidth outputs. The signals were non-return-to-zero shaped; no digital pulse shaping was applied. The data was modulated onto five external cavity lasers (ECLs) with less than 100-kHz linewidths using an InP IQ modulator (IQM) with 35-GHz electro-optical bandwidth to create five 28-Gbaud, single-polarization 16QAM channels. PDM was emulated using a polarization-maintaining 3-dB coupler with a length of polarization-maintaining fiber on one output, which caused a delay of about 286 symbols. The signal and its delayed copy were then re-combined in a PBC to create a PDM signal. The channels were then de-correlated using a fiber Bragg grating (FBG) channelized dispersion compensating module (DCM) and 80 km of SMF-28e. The dispersion of the SMF introduced a group delay of approximately 16 symbols

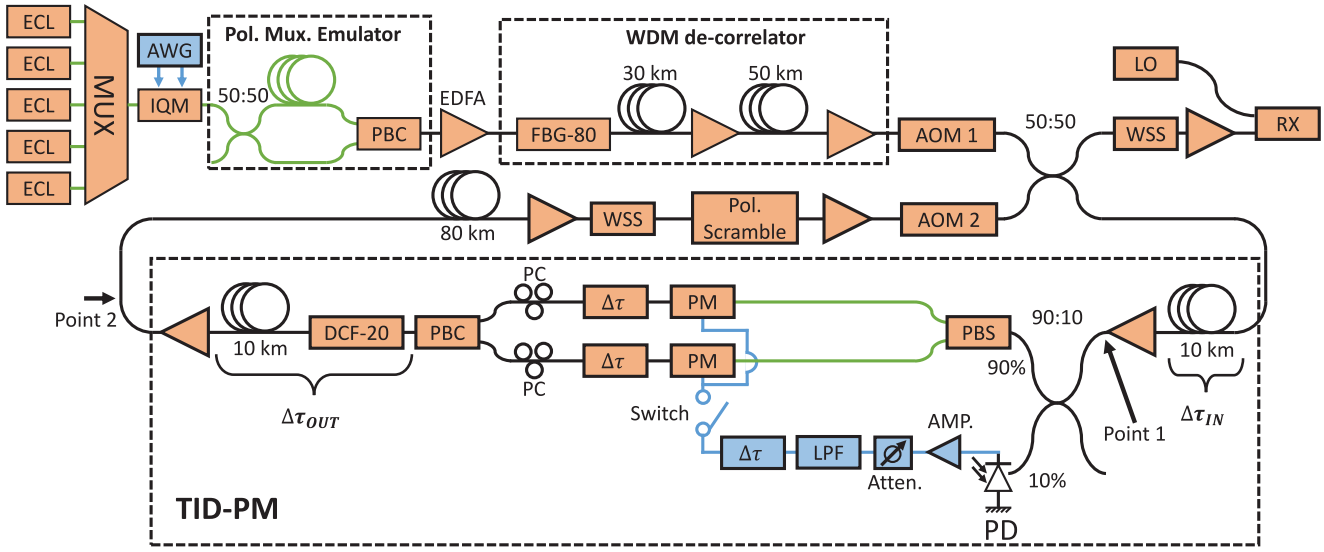

Fig. 16. Experimental setup of an 800-km, WDM link with in-line TID-PMs. ECL: External cavity laser; IQM: 35-GHz bandwidth IQ modulator; AWG: Arbitrary waveform generator; PBC: Polarization beam combiner; FBG-80: Fiber Bragg grating-based channelized dispersion compensating module for 80-km of SMF-28e; AOM: Acousto-optic modulator (used for re-circulating loop); PD: Photodiode; Amp.: Electrical amplifier; Atten: Electrical attenuator; LPF: Electrical low-pass filter; $\Delta\tau$: Variable delay (blue: electrical; orange: optical); PBS: Polarization beam splitter; PM: Phase Modulator; PC: polarization controller; DCF-20: Dispersion-compensating fiber for 20-km of SMF-28e; WSS: Wavelength-selective switch; Pol. Scramble: Polarization scrambler; LO: Local oscillator laser; RX: Coherent receiver. Green lines indicate polarization-maintaining fiber, and blue lines are electrical connections. From [58].

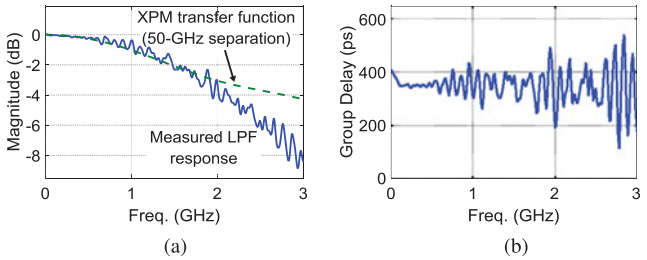

Fig. 17. (a) Measured (blue) and desired (green) frequency response and (b) measured group delay of the Mini-Circuits SBLP-1870+ filter used in the TID-PM prototype.

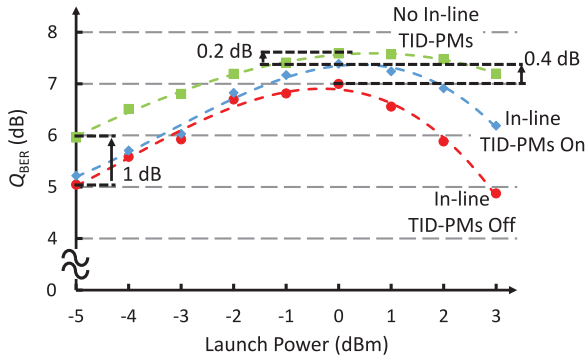

Fig. 18. Experimental Q_{BER} *vs.* per-channel launch power for the center PDM-16QAM channel after 800-km transmission with in-line TID-PMs turned on (blue), in-line TID-PMs turned off (red), and no in-line TID-PMs (green). From [58].

between adjacent channels. The channelized DCM compensated the pulse-spreading of each channel without affecting the inter-channel walk-off. To minimize the OSNR penalty caused by the de-correlator, an EDFA was placed after the first 30-km span. The WDM signal was then launched into a recirculating loop.

The 5-channel PDM-16QAM signal traversed the loop ten times before exiting, at which point the center channel was de-multiplexed with a 40-GHz WSS, pre-amplified to -1 dBm, and then coherently detected on a 25-GHz bandwidth coherent receiver. The electrical outputs were then sampled with an 80-GSa/s, 33-GHz bandwidth real-time sampling oscilloscope and stored for off-line processing. Post-processing involved down-sampling to 2 samples per symbol, frequency offset compensation using spectral-peak search, and electronic dispersion compensation using the overlap-add algorithm. Equalization and polarization de-multiplexing were achieved using a 2-stage constant-modulus algorithm (CMA) equalizer: the first stage, a single-ring CMA, initialized the digital filter taps for the second stage, a radial decision-directed CMA, to fully recover the 16QAM constellation. After equalization, phase noise was removed via a maximum likelihood algorithm, and the BER was estimated using direct error counting. This was then converted to Q_{BER} using (10).

Fig. 18 plots Q_{BER} against per-channel launch power for the center channel with in-line TID-PMs turned off (red circles), i.e., not mitigating fiber nonlinearity, and turned on (blue diamonds), i.e., mitigating the nonlinear distortion. We also plot the curve for the link without in-line TID-PMs (green squares) for reference. Each marker is the average of 10 measurements, and the dashed lines are plotted as guidelines. While enabling NLC results in a 0.4-dB improvement in peak Q_{BER}, the optimum launch power remains at 0 dBm in both cases. Comparing system performance with and without TID-PMs, there is a 1-dB OSNR penalty at -5 dBm; assuming the 80-km span has a loss of 16 dB and the EDFAs have 6-dB NFs, the expected OSNR penalty is 1.2 dB. However, this results in a 0.6-dB penalty at peak Q_{BER},

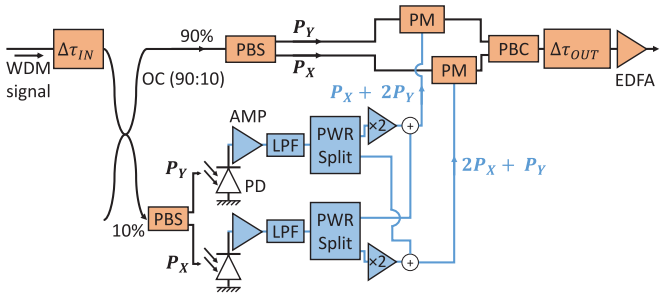

Fig. 19. Block diagram of a polarization-diverse TID-PM that applies different phase rotations to each polarization.

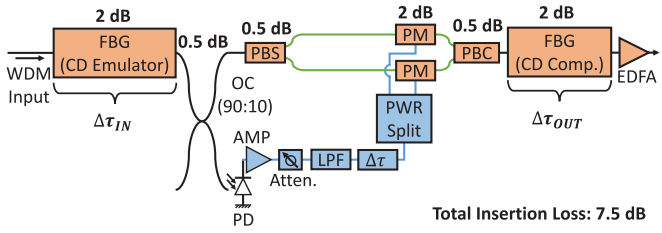

Fig. 20. Block diagram of a TID-PM with reduced insertion loss, where the estimated loss of each element is labeled. The green lines indicate polarization-maintaining fiber, and the blue lines indicate electrical connections.

which is not overcome by the 0.4-dB improvement from using in-line TID-PMs. Therefore, in-line TID-PMs cause a net performance penalty in this case. Further, the link with TID-PMs has an increased nonlinear distortion in the high-power region, which is attributed to additional nonlinear distortions that are generated in the SMF and DCF used for $\Delta\tau_{IN/OUT}$.

We note that the performance improvement observed experimentally is smaller than the value predicted in simulation. We attribute this to the group delay ripple on the LPF [Fig. 17(b)], which causes a frequency-dependent path mis-match between the electrical and optical pulses. As we showed in Fig. 11, this can result in a significant reduction in TID-PM effectiveness. Additionally, while this experiment aims to compensate both SPM and XPM, we have not quantified how effectively each impairment is mitigated. Therefore, it is possible that only a small amount of XPM is compensated in this case. However, we have previously demonstrated effective XPM mitigation using a TID-PM in [57].

V. Discussion

While our investigations show that in-line TID-PMs are able to mitigate fiber nonlinearity in particular systems, there are many areas that need further attention. Several of these relate to the optimization of TID-PMs, while others concern their use in long-haul transmission systems. As previously described in Section II, we implemented a polarization-diverse TID-PM using a single electrical arm. However, given that we use two phase modulators, there may be some benefit to applying different phase rotations in each arm to account for the relative strengths of XPM and SPM contributions from each polarization. This would involve the use of two electrical arms, and a cross-connect between them, as shown in Fig. 19. It should be noted that the power contribution from individual WDM channels cannot be separated, meaning that there will always be some over- or under-compensation. However, in situations where XPM is more significant than SPM, there may be some value in optimizing the contributions from each polarization tributary. Alternatively, the development of a low-loss polarization-insensitive phase modulator could further simplify the original design.

One critical area that was highlighted by the proof-of-concept experiment in Section IV is the insertion loss of the TID-PM. This caused a large OSNR penalty, and led to a net reduction in system performance despite nonlinearity mitigation. While we measured an insertion loss of 11.2 dB for this prototype, there were several components that we were forced to use by necessity, e.g., the second 10-km spool of SSMF to balance the 20 km-equivalent DCF. We believe that it may be possible to reduce the insertion loss to around 7.5 dB using commercially available components, as shown in Fig. 20. Ultra-low loss phase modulators that achieve 2-dB insertion loss by trading off V_π and modulator bandwidth are commercially available, and it may be possible to replace the SMF and DCF for the $\Delta\tau_{IN/OUT}$ elements with FBGs that have insertion losses in the region of 2 dB. These FBGs would apply a small amount of dispersion over a wide bandwidth. Alternatively, it may be possible to eliminate the OSNR penalty by removing the EDFA from the TID-PM, and instead increasing the launch power into the device. Using a simple calculation, it can easily be shown that the OSNR penalty from an increased span loss can be mitigated by increasing the launch power into the system. Therefore, if the signal is launched into the TID-PM at the desired launch power into the fiber span plus the insertion loss of the TID-PM, this would technically introduce no net OSNR penalty. Of course, this calculation does not apply to systems limited by fiber nonlinearity, and so is only valid if the TID-PM does not introduce additional nonlinear distortions.

Another open area for study is how to best emulate the XPM transfer functions of several WDM channels. We mainly considered a LPF with a 0.5-order Gaussian profile because this was found to be optimal for filtered DBP [77], and did not try and iterate on this further. However, we have no reason to believe that this is the optimal case when compensating both SPM and XPM, and so optimization of the LPF parameters may enable better system performance, particularly when XPM is the dominant impairment. Further, deriving an analytic, or semi-analytic, way to optimize the LPF and optical group delay parameters based on system design parameters could be very beneficial.

Fundamentally, the performance of the TID-PM approach will be limited by the approximation of modeling nonlinear distortions as a discrete phase rotation over a span of optical fiber. This neglects higher order mixing terms such as FWM and XpolM, and wider bandwidth components of effects such as SPM and signal-ASE nonlinear mixing. Neglecting these effects has been shown to be a limiting factor for DBP [49], and so we can expect that TID-PMs have similar basic limitations. To push performance beyond these limits would suggest that a more complex in-line nonlinearity compensation scheme is

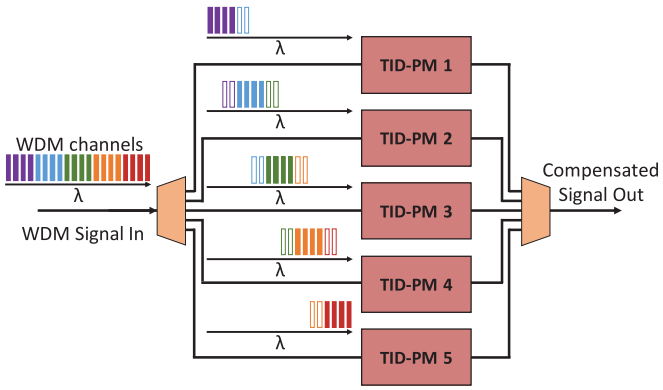

Fig. 21. Proposed method to achieve broadband NLC using spectral slicing and a bank of TID-PMs. The solid (center) channels in each slice are compensated, while the open (edge) channels are included in the estimate of the nonlinear distortion on the center channels but are not compensated. From [50].

required, specifically a sub-system that is capable of mitigating wide-band effects, such as a system based on cascaded OPC. We also note that to date the largest increase in transmission reach has been provided by digital pre-compensation of nonlinearities [48], and so for the highest performance links, there may be a need to trade-off flexible optical network design.

Looking towards more practical issues for in-line TID-PMs, an additional area of study is the compensation of signals containing large numbers of WDM channels. In our investigations, we only considered the nonlinear distortion affecting channels in a small part of the available bandwidth of an optical system, but ideally we would want to be able to mitigate all channels in the C-band. However, using a single TID-PM to compensate XPM over a much broader bandwidth than we explore here is expected to be ineffective. Essentially, the XPM transfer functions for spectrally close and distant channels can be significantly different [see (6)], and so using one 'average' electrical filter in the TID-PM is unlikely to accurately model the impact of differing amounts of walk-off between channels. This will result in over- and/or under-compensation of XPM between different pairs of channels, which should significantly reduce the efficacy of in-line TID-PMs. A possible solution to this problem is to slice the spectrum into bands of WDM channels, and use a TID-PM on each band, as shown in Fig. 21 [50]. Further, this may enable a level of flexibility when dealing with channels that have non-uniform baud rates and frequency spacings. As long as the channels near the center of each band have the same properties, the parameters of the TID-PM in each band can be adjusted to optimize performance.

VI. Conclusion

In conclusion, we have presented a review of our work on nonlinearity compensation using optoelectronic sub-systems placed in-line with the fiber link. These sub-systems, called 'total intensity-directed phase modulators' (TID-PMs), use low-bandwidth components and can mitigate the distortion caused by SPM and XPM over several WDM channels. We explained how walk-off attenuates the XPM distortion in long-haul links, and showed that a significant portion of the remaining distortion is caused by low-frequency intensity fluctuations. We then showed, via numerical simulation, that TID-PMs placed in-line with the fiber link can be used to mitigate these low-frequency components and enable a significant performance improvement. Further simulations demonstrated that in-line TID-PMs are compatible with polarization-division-multiplexed signals and optical routing, and can enable greater performance improvements than single-channel DBP with one-step-per-span. From a practical stand-point, in-line TID-PMs can tolerate small errors in phase modulation depth and path-length matching between the electrical and optical arms. We also performed a proof-of-concept experiment, and showed that in-line TID-PMs were able to mitigate the nonlinear distortion on a 5-channel, 28-Gbaud PDM-16QAM signal transmitted through an 800-km dispersion unmanaged link. While in-line TID-PMs are not able to fully compensate the distortion caused by fiber nonlinearity, they can enable significant improvements to system performance using relatively low-bandwidth components. Therefore, further work in optoelectronic sub-systems may result in a relatively simple way to mitigate a significant portion of the nonlinear distortion in long-haul optical fiber links.

Acknowledgment

The authors would like to thank Prof. A. D. Ellis of Aston University and Prof. P. J. Winzer of Nokia Bell Labs for their comments on the thesis that this work is based on. The authors would also like to thank VPIphotonics for supporting the use of VPItransmissionMaker under their universities program.

References

[1] P. P. Mitra and J. B. Stark, "Nonlinear limits to the information capacity of optical fibre communications," *Nature*, vol. 411, no. 6841, pp. 1027–1030, 2001.

[2] R.-J. Essiambre, G. J. Foschini, G. Kramer, and P. J. Winzer, "Capacity limits of information transport in fiber-optic networks," *Phys. Rev. Lett.*, vol. 101, no. 16, 2008, Art. no. 163901.

[3] A. D. Ellis, J. Zhao, and D. Cotter, "Approaching the non-linear Shannon limit," *J. Lightw. Technol.*, vol. 28, no. 4, pp. 423–433, Feb. 2010.

[4] E. Ip and J. M. Khan, "Compensation of dispersion and nonlinear impairments using digital backpropagation," *J. Lightw. Technol.*, vol. 26, no. 20, pp. 3416–3425, Oct. 2008.

[5] X. Li *et al.*, "Electronic post-compensation of WDM transmission impairments using coherent detection and digital signal processing," *Opt. Express*, vol. 16, no. 2, pp. 880–888, Jan. 2008.

[6] E. Ip, "Nonlinear compensation using backpropagation for polarization-multiplexed transmission," *J. Lightw. Technol.*, vol. 28, no. 6, pp. 939–951, Mar. 2010.

[7] E. Temprana *et al.*, "Overcoming Kerr-induced capacity limit in optical fiber transmission," *Science*, vol. 348, no. 6242, pp. 1445–1448, 2015.

[8] E. Temprana *et al.*, "Two-fold transmission reach enhancement enabled by transmitter-side digital backpropagation and optical frequency comb-derived information carriers," *Opt. Express*, vol. 23, no. 16, pp. 20774–20783, 2015.

[9] L. B. Du and A. J. Lowery, "Improved single channel backpropagation for intra-channel fiber nonlinearity compensation in long-haul optical communication systems," *Opt. Express*, vol. 18, no. 16, pp. 17075–17088, 2010.

[10] D. Rafique, M. Mussolin, M. Forzati, J. Martensson, M. N. Chugtai, and A. D. Ellis, "Compensation of intra-channel nonlinear fibre impairments using simplified digital back-propagation algorithm," *Opt. Express*, vol. 19, no. 10, pp. 9453–9460, 2011.

[11] X. Liang and S. Kumar, "Multi-stage perturbation theory for compensating intra-channel nonlinear impairments in fiber-optic links," *Opt. Express*, vol. 22, no. 24, pp. 29733–29745, 2014.

[12] X. Liang, S. Kumar, J. Shao, M. Malekiha, and D. V. Plant, "Digital compensation of cross-phase modulation distortions using perturbation technique for dispersion-managed fiber-optic systems," *Opt. Express*, vol. 22, no. 17, pp. 20 634–20 645, Aug. 2014.

[13] X. Liang and S. Kumar, "Correlated digital back propagation based on perturbation theory," *Opt. Express*, vol. 23, no. 11, pp. 14655–14665, Jun. 2015.

[14] S. T. Le, I. D. Philips, J. E. Prilepsky, P. Harper, A. D. Ellis, and S. K. Turitsyn, "Demonstration of nonlinear inverse synthesis transmission over transoceanic distances," *J. Lightw. Technol.*, vol. 34, no. 10, pp. 2459–2466, May 2016.

[15] S. T. Le, J. E. Prilepsky, P. Rosa, J. D. Ania-Castan, and S. K. Turitsyn, "Nonlinear inverse synthesis for optical links with distributed Raman amplification," *J. Lightw. Technol.*, vol. 34, no. 8, pp. 1778–1786, Apr. 2016.

[16] S. T. Le and H. Buelow, "64 × 0.5 Gbaud nonlinear frequency division multiplexed transmissions with high order modulation formats," *J. Lightw. Technol.*, vol. 35, no. 17, pp. 3692–3698, Sep. 2017.

[17] B. Inan, S. Randel, S. L. Jansen, A. Lobato, S. Adhikari, and N. Hanik, "Pilot-tone-based nonlinearity compensation for optical OFDM systems," in *Proc. 36th Eur. Conf. Exhib. Opt. Commun.*, 2010, Paper Tu.4.A.6.

[18] L. B. Du and A. J. Lowery, "Pilot-based cross-phase modulation compensation for coherent optical orthogonal frequency division multiplexing long-haul optical communications systems," *Opt. Lett.*, vol. 36, no. 9, pp. 1647–1649, 2011.

[19] L. B. Du and A. J. Lowery, "Pilot-based XPM nonlinearity compensator for CO-OFDM systems," *Opt. Express*, vol. 19, no. 26, pp. B862–B867, 2011.

[20] A. Diaz *et al.*, "Analysis of back-propagation and RF pilot-tone based nonlinearity compensation for a 9 × 224 Gb/s POLMUX-16QAM system," in *Proc. Opt. Fiber Commun. Conf. Expo./Nat. Fiber Opt. Eng. Conf.*, 2012, Paper OTh3C.5.

[21] X. Liu, A. R. Chraplyvy, P. J. Winzer, R. W. Tkach, and S. Chandrasekhar, "Phase-conjugated twin waves for communication beyond the Kerr nonlinearity limit," *Nature Photon.*, vol. 7, no. 7, pp. 560–568, 2013.

[22] X. Liu, S. Chandrasekhar, P. J. Winzer, R. W. Tkach, and A. R. Chraplyvy, "Fiber-nonlinearity-tolerant superchannel transmission via nonlinear noise squeezing and generalized phase-conjugated twin waves," *J. Lightw. Technol.*, vol. 32, no. 4, pp. 766–775, Feb. 2014.

[23] C. Xu and X. Liu, "Postnonlinearity compensation with data-driven phase modulators in phase-shift keying transmission," *Opt. Lett.*, vol. 27, no. 18, pp. 1619–1621, 2002.

[24] A. J. Lowery, "Fiber nonlinearity mitigation in optical links that use OFDM for dispersion compensation," *IEEE Photon. Technol. Lett.*, vol. 19, no. 19, pp. 1556–1558, 2007.

[25] A. J. Lowery, "Fiber nonlinearity pre- and post-compensation for long-haul optical links using OFDM," *Opt. Express*, vol. 15, no. 20, pp. 12965–12970, Oct. 2007.

[26] K. Kikuchi, "Electronic post-compensation for nonlinear phase fluctuations in a 1000-km 20-Gbit/s optical quadrature phase-shift keying transmission system using the digital coherent receiver," *Opt. Express*, vol. 16, no. 2, pp. 889–896, 2008.

[27] L. B. Du and A. J. Lowery, "Practical XPM compensation method for coherent optical OFDM systems," *IEEE Photon. Technol. Lett.*, vol. 22, no. 5, pp. 320–322, Mar. 2010.

[28] L. Du and A. Lowery, "Experimental demonstration of XPM compensation for CO-OFDM systems with periodic dispersion maps," in *Proc. Opt. Fiber Commun. Conf. Expo./Nat. Fiber Opt. Eng. Conf.*, Mar. 2011, Paper OWW2.

[29] S. L. Jansen *et al.*, "16 × 40 Gb/s over 800 km of SSMF using mid-link spectral inversion," *IEEE Photon. Technol. Lett.*, vol. 16, no. 7, pp. 1763–1765, Jul. 2004.

[30] L. Du, M. M. Morshed, and A. J. Lowery, "Fiber nonlinearity compensation for OFDM super-channels using optical phase conjugation," *Opt. Express*, vol. 20, no. 18, pp. 19921–19927, 2012.

[31] I. D. Phillips *et al.*, "Exceeding the nonlinear-Shannon limit using Raman laser based amplification and optical phase conjugation," in *Proc. Opt. Fiber Commun. Conf. Exhib.*, 2014, Paper M3C.1.

[32] M. Morshed, L. B. Du, B. Foo, M. D. Pelusi, B. Corcoran, and A. J. Lowery, "Experimental demonstrations of dual polarization CO-OFDM using mid-span spectral inversion for nonlinearity compensation," *Opt. Express*, vol. 22, no. 9, pp. 10455–10466, 2014.

[33] A. D. Ellis *et al.*, "4 Tb/s transmission reach enhancement using 10 × 400 Gb/s super-channels and polarization insensitive dual band optical phase conjugation," *J. Lightw. Technol.*, vol. 34, no. 8, pp. 1717–1723, Apr. 2016.

[34] M. H. Shoreh, "Compensation of nonlinearity impairments in coherent optical OFDM systems using multiple optical phase conjugate modules," *IEEE/OSA J. Opt. Commun. Netw.*, vol. 6, no. 6, pp. 549–558, Jun. 2014.

[35] A. D. Ellis, M. E. McCarthy, M. A. Z. Al-Khateeb, and S. Sygletos, "Capacity limits of systems employing multiple optical phase conjugators," *Opt. Express*, vol. 23, no. 16, pp. 20381–20393, 2015.

[36] A. Ellis, M. Al-Khateeb, and M. McCarthy, "Impact of optical phase conjugation on the nonlinear Shannon limit," *J. Lightw. Technol.*, vol. 35, no. 4, pp. 792–798, Feb. 2017.

[37] K. Solis-Trapala, M. Pelusi, H. N. Tan, T. Inoue, and S. Namiki, "Optimized WDM transmission impairment mitigation by multiple phase conjugations," *J. Lightw. Technol.*, vol. 34, no. 2, pp. 431–440, Jan. 2016.

[38] S. Namiki, K. Solis-Trapala, H. N. Tan, M. Pelusi, and T. Inoue, "Multi-channel cascadable parametric signal processing for wavelength conversion and nonlinearity compensation," *J. Lightw. Technol.*, vol. 35, no. 4, pp. 815–823, Feb. 2017.

[39] H. Hu *et al.*, "Fiber nonlinearity compensation of an 8-channel WDM PDM-QPSK signal using multiple phase conjugations," in *Proc. Opt. Fiber Commun. Conf. Exhib.*, 2014, Paper M2C.2.

[40] H. Hu, R. M. Jopson, A. H. Gnauck, D. Pilori, S. Randel, and S. Chandrasekhar, "Fiber nonlinearity compensation by repeated phase conjugation in 2.048-Tbit/s WDM transmission of PDM 16-QAM channels," in *Proc. Opt. Fiber Commun. Conf. Exhib.*, Mar. 2016, Paper Th4F.3.

[41] H. Hu, R. M. Jopson, A. H. Gnauck, S. Randel, and S. Chandrasekhar, "Fiber nonlinearity mitigation of WDM-PDM QPSK/16-QAM signals using fiber-optic parametric amplifiers based multiple optical phase conjugations," *Opt. Express*, vol. 25, no. 3, pp. 1618–1628, Feb. 2017.

[42] S. L. I. Olsson, B. Corcoran, C. Lundstrm, T. A. Eriksson, M. Karlsson, and P. A. Andrekson, "Phase-sensitive amplified transmission links for improved sensitivity and nonlinearity tolerance," *J. Lightw. Technol.*, vol. 33, no. 3, pp. 710–721, Feb. 2015.

[43] H. Eliasson, S. L. I. Olsson, M. Karlsson, and P. A. Andrekson, "Mitigation of nonlinear distortion in hybrid Raman/phase-sensitive amplifier links," *Opt. Express*, vol. 24, no. 2, pp. 888–900, Jan. 2016.

[44] J. Shao and S. Kumar, "Optical backpropagation for fiber-optic communications using optical phase conjugation at the receiver," *Opt. Lett.*, vol. 37, no. 15, pp. 3012–3014, 2012.

[45] X. Liang, S. Kumar, and J. Shao, "Ideal optical backpropagation of scalar NLSE using dispersion-decreasing fibers for WDM transmission," *Opt. Express*, vol. 21, no. 23, pp. 28668–28675, 2013.

[46] X. Liang and S. Kumar, "Optical back propagation for compensating nonlinear impairments in fiber optic links with ROADMs," *Opt. Express*, vol. 24, no. 20, pp. 22 682–22 692, Oct. 2016.

[47] X. Liang and S. Kumar, "Optical back propagation for fiber optic networks with hybrid EDFA Raman amplification," *Opt. Express*, vol. 25, no. 5, pp. 5031–5043, Mar. 2017.

[48] E. Temprana *et al.*, "Demonstration of coherent transmission reach tripling by frequency-referenced nonlinearity pre-compensation in EDFA-only SMF link," in *Proc. Eur. Conf. Exhib. Opt. Commun.*, Sep. 2016, pp. 376–378.

[49] R. Dar and P. J. Winzer, "Nonlinear interference mitigation: Methods and potential gain," *J. Lightw. Technol.*, vol. 35, no. 4, pp. 903–930, Feb. 2017.

[50] B. Foo, B. Corcoran, C. Zhu, and A. J. Lowery, "Distributed nonlinearity compensation of dual-polarization signals using optoelectronics," *IEEE Photon. Technol. Lett.*, vol. 28, no. 20, pp. 2141–2144, Oct. 2016.

[51] M. E. McCarthy, M. A. Z. A. Kahteeb, F. M. Ferreira, and A. D. Ellis, "PMD tolerant nonlinear compensation using in-line phase conjugation," *Opt. Express*, vol. 24, no. 4, pp. 3385–3392, Feb. 2016.

[52] D. Rafique and A. D. Ellis, "Impact of signal-ASE four-wave mixing on the effectiveness of digital back-propagation in 112 Gb/s PM-QPSK systems," *Opt. Express*, vol. 19, no. 4, pp. 3449–3454, 2011.

[53] G. Gao, X. Chen, and W. Shieh, "Influence of PMD on fiber nonlinearity compensation using digital back propagation," *Opt. Express*, vol. 20, no. 13, pp. 14406–14418, 2012.

[54] K. Solis-Trapala, T. Inoue, and S. Namiki, "Nearly-ideal optical phase conjugation based nonlinear compensation system," in *Proc. Opt. Fiber Commun. Conf. Exhib.*, Mar. 2014, Paper W3F.8.

[55] K. Solis-Trapala, T. Inoue, and S. Namiki, "Signal power asymmetry tolerance of an optical phase conjugation-based nonlinear compensation system," in *Proc. Eur. Conf. Exhib. Opt. Commun.*, Sep. 2014, Paper We.2.5.4.
[56] B. Foo, B. Corcoran, and A. Lowery, "Optoelectronic method for inline compensation of XPM in long-haul optical links," *Opt. Express*, vol. 23, no. 2, pp. 859–872, 2015.
[57] B. Foo, B. Corcoran, and A. Lowery, "Compensating XPM using a low-bandwidth phase modulator," *IEEE Photon. Technol. Lett.*, vol. 29, no. 9, pp. 699–702, May 2017.
[58] B. Foo, B. Corcoran, and A. Lowery, "Demonstration of DP-16QAM WDM link with in-line nonlinearity compensation," in *Proc. Opto-Electron. Commun. Conf. Photonics Global Conf.*, Aug. 2017, pp. 1–3.
[59] A. Lowery and B. Foo, "Distributed nonlinear compensation using optoelectronic circuits," in *Proc. Eur. Conf. Exhib. Opt. Commun.*, Sep. 2017, Paper W.2.E.2.
[60] D. Marcuse, C. R. Manyuk, and P. K. A. Wai, "Application of the Manakov-PMD equation to studies of signal propagation in optical fibers with randomly varying birefringence," *J. Lightw. Technol.*, vol. 15, no. 9, pp. 1735–1746, Sep. 1997.
[61] C. R. Menyuk and B. S. Marks, "Interaction of polarization mode dispersion and nonlinearity in optical fiber transmission systems," *J. Lightw. Technol.*, vol. 24, no. 7, pp. 2806–2826, Jul. 2006.
[62] G. Agrawal, *Nonlinear Fiber Optics*. San Diego, CA, USA: Academic, 2013.
[63] F. Tappert, "Numerical solutions of the Korteweg-de Vries equation and its generalizations by the split-step Fourier method," *Nonlinear Wave Motion*, vol. 15, pp. 215–216, 1974.
[64] N. Shibata, R. Braun, and R. Waarts, "Phase-mismatch dependence of efficiency of wave generation through four-wave mixing in a single-mode optical fiber," *IEEE J. Quantum Electron.*, vol. QE-23, no. 7, pp. 1205–1210, Jul. 1987.
[65] A. Bononi, N. Rossi, and P. Serena, "Transmission limitations due to fiber nonlinearity," in *Proc. Opt. Fiber Commun. Conf. Expo./Nat. Fiber Opt. Eng. Conf.*, Mar. 2011, Paper OWO7.
[66] C. Xie, "Impact of nonlinear and polarization effects in coherent systems," *Opt. Express*, vol. 19, no. 26, pp. B915–B930, Dec. 2011.
[67] N. Rossi, P. Serena, and A. Bononi, "Symbol-rate dependence of dominant nonlinearity and reach in coherent WDM links," *J. Lightw. Technol.*, vol. 33, no. 14, pp. 3132–3143, Jul. 2015.
[68] E. F. Mateo, X. Zhou, and G. Li, "Improved digital backward propagation for the compensation of inter-channel nonlinear effects in polarization-multiplexed WDM systems," *Opt. Express*, vol. 19, no. 2, pp. 570–583, 2011.
[69] D. Marcuse, A. R. Chraplyvy, and R. W. Tkach, "Dependence of cross-phase modulation on channel number in fiber WDM systems," *J. Lightw. Technol.*, vol. 12, no. 5, pp. 885–890, May 1994.
[70] T.-K. Chiang, N. Kagi, T. K. Fong, M. E. Marhic, and L. G. Kazovsky, "Cross-phase modulation in dispersive fibers: Theoretical and experimental investigation of the impact of modulation frequency," *IEEE Photon. Technol. Lett.*, vol. 6, no. 6, pp. 733–736, Jun. 1994.
[71] T.-K. Chiang, N. Kagi, M. E. Marhic, and L. G. Kazovsky, "Cross-phase modulation in fiber links with multiple optical amplifiers and dispersion compensators," *J. Lightw. Technol.*, vol. 14, no. 3, pp. 249–260, Mar. 1996.
[72] Z. Tao *et al.*, "Simple fiber model for determination of XPM effects," *J. Lightw. Technol.*, vol. 29, no. 7, pp. 974–986, Apr. 2011.
[73] X. Liang and S. Kumar, "Analytical modeling of XPM in dispersion-managed coherent fiber-optic systems," *Opt. Express*, vol. 22, no. 9, pp. 10579–10592, May 2014.
[74] Y. Fan, L. Dou, Z. Tao, T. Hoshida, and J. C. Rasmussen, "A high performance nonlinear compensation algorithm with reduced complexity based on XPM model," in *Proc. Opt. Fiber Commun. Conf. Exhib.*, Mar. 2014, Paper Th2A.8.
[75] F. Zhang, Q. Zhuge, M. Qiu, W. Wang, M. Chagnon, and D. V. Plant, "XPM model-based digital backpropagation for subcarrier-multiplexing systems," *J. Lightw. Technol.*, vol. 33, no. 24, pp. 5140–5150, Dec. 2015.
[76] L. B. Du and A. J. Lowery, "Improved nonlinearity precompensation for long-haul high-data-rate transmission using coherent optical OFDM," *Opt. Express*, vol. 16, no. 24, pp. 19920–19925, 2008.
[77] I. F. d. J. Ruiz, A. Ghazisaeidi, and G. Charlet, "Optimization rules and performance analysis of filtered digital backpropagation," in *Proc. Eur. Conf. Exhib. Opt. Commun.*, 2015, pp. 1–3.
[78] A. Ghazisaeidi *et al.*, "Submarine transmission systems using digital nonlinear compensation and adaptive rate forward error correction," *J. Lightw. Technol.*, vol. 34, no. 8, pp. 1886–1895, Apr. 2016.

Benjamin Foo (S'15) received the B.Eng. degree (first class Hons.) in electrical and computer systems engineering and the Ph.D. degree from Monash University, Melbourne, VIC, Australia. During the Ph.D. degree, he worked on an optoelectronic method for nonlinearity compensation in long-haul optical communication systems. In mid-2017, he joined Chalmers University of Technology, Gothenburg, Sweden, as a Postdoctoral Researcher, where he is currently working on phase-sensitive amplifiers and their applications. His current research interests include fiber nonlinearity compensation, high-throughput optical communication systems, and digital and optical signal processing.

Bill Corcoran (S'08–M'11) received the B.Sc. degree in physics and the B.Eng. degree (Hons.) from RMIT University, Melbourne, VIC, Australia, in 2006, and the Ph.D. degree in physics from the University of Sydney, Sydney, NSW, Australia, where he investigated the properties of slow light and optical nonlinearities in silicon waveguide structures, and their applications to all-optical signal processing. From 2011 to 2013, he was a Postdoctoral Research Fellow with the Photonics Laboratory, Chalmers University of Technology, Gothenburg, Sweden, where he investigated the use of optical phase-sensitive amplifiers in fiber communications systems for both low noise amplification and the compensation of optical nonlinear distortions. In 2013, he joined the Electro-Photonics Laboratory, Monash University, Melbourne, VIC, Australia, where he worked on fiber subsystems and signal processing for fiber communication systems, and as a Project Leader of the Terabit-per-Second flagship for the ARC Centre of Excellence in Ultrahigh-Bandwidth Devices for Optical Systems. In 2015, he was made an ongoing member of staff within the Department of Electrical and Computer Systems Engineering, Monash University. Summaries of his research can be found at https://orcid.org/0000-0001-8653-3999 and https://scholar.google.com.au/citations?user=8Qbd_OAAAAAJ&hl=en&oi= ao.

Arthur J. Lowery (M'92–SM'96–F'09) was born in Yorkshire, U.K., in 1961. He received the B.Sc. degree (first class Hons.) in applied physics from the University of Durham, Durham, U.K., in 1983, and the Ph.D. degree in electrical and electronic engineering from the University of Nottingham, Nottingham, U.K., in 1988. From 1983 to 1984, he was with Marconi Radar Systems Ltd., U.K. In 1984, he joined the University of Nottingham as a Lecturer and pioneered time-domain field modeling of semiconductor lasers as the transmission-line laser model. In 1990, he joined the University of Melbourne, Australia. In 1996, he cofounded the Virtual Photonics Pty. Ltd. (now VPIphotonics) and led to the development of VPIs physical-level photonic design automation tools, such as OPALS, VPItransmissionMaker, and VPIcomponentMaker. In 2004, he was appointed as a Professor with the Department of Electrical and Computer Systems Engineering, Monash University, Melbourne, VIC, Australia, and was the Head between 2007 and 2012. In 2008, he founded Ofidium to commercialize optical OFDM for long-haul systems. In 2009, he was elected an IEEE Fellow for leadership in computer modeling of optical communication systems. He is currently the Director of the Monash Vision Group's Cortical-Implant Bionic Eye project and Science Leader of Tbit/s Systems in the ARC's Centre of Excellence in Ultrahigh-Bandwidth Devices for Optical Systems, and a Chief Investigator with the Centre for Integrative Brain Function. He has authored/coauthored more than 350 papers. He is a Fellow of the ATSE. He was a recipient of a five-year ARC Laureate Fellowship to work on electro-photonic interchanges in 2013.